Catalysis Science & Technology

Accepted Manuscript

ROYAL SOCIETY OF CHEMISTRY

www.rsc.org/catalysis

Journal Name

RSCPublishing

ARTICLE

Short-time chemical looping on magnetite material for hydrogen production from bio-ethanol

Cite this: DOI: 10.1039/xoxxoooooox

C. Trevisanut[a,b], F. Bosselet[b], F. Cavani[a] and J. M. M. Millet[b*]

Received ooth January 2012,
Accepted ooth January 2012

DOI: 10.1039/xoxxoooooox

www.rsc.org/

Magnetite samples were synthesized and studied as the cycling material of a chemical loop process for hydrogen production from ethanol and water used as reducing and oxidizing species, respectively. Surface and structural changes during the process were characterized by various techniques such as X-ray diffraction, X-ray photoelectron, and Mössbauer spectroscopy in order to evidence the real cycling process and understand the cause of the material deactivation so it can be suppressed or minimized for an industrial application. We found that the complete recovery of the initial cycling material was possible, but that a slow accumulation of coke took place over time under cycling conditions. Indeed, this deposited coke corresponds to only a part of the coke formed, since water makes partial re-oxidation possible. A third step to burn the coke left over by the air will thus have to be periodically added for a sustainable industrial process, unless a cycling material and/or certain conditions capable of either totally preventing the formation of coke or leading to the formation of coke that is not oxidized by water are found.

1. Introduction

Steam reforming of bio-alcohol offers an attractive route for H_2 production from renewable sources. In addition to being environmentally friendly, it has the potential of being carbon neutral and is amenable to a local distributed energy generation strategy. Because of these advantages, many studies focusing on such a process in different catalytic systems have been conducted. Although high-performance catalysts have been proposed, H_2 production must be enhanced and catalyst deactivation problems solved. One way to overcome these technological stumbling blocks is to use an alternative reaction-engineering concept based upon a chemical loop.

This approach consists of a two-step process: first the reduction of an oxide by a reducer followed by water splitting at the same temperature, thus leading to H_2 production and the correlative re-oxidation of the material (Scheme 1).

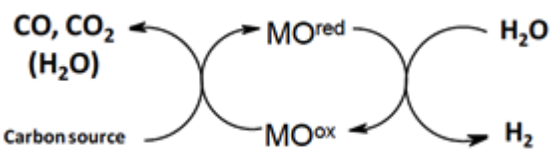

Scheme 1: Key principle of the chemical looping for H_2 production

These cycles have been the focus of constant attention over the past twenty years and various reducers have been studied.[1-6] Numerous papers have been published on the gasified coal conversion with this process because it allows a control of the CO_2 formed and it makes possible successive captute.[7-9] However methane has also extensively been studied as reducer.[9,10] If perowskite-type materials have been shown to be efficient in all these cases,[11-14] magnetite may have at the present time, got the upper hand because of its performances, lost cost and begnin ecological impact.[15-17] It has been used pure or in mixture with other oxides[18,19] or concomitantly with oxygen permeable ceramic to improve H_2 separation.[20] Recently, light alcohols such as ethanol, which offers all the advantages of being a renewable feedstock produced in large quantities and does not call for high reforming temperature, have been selected as possible reducers, and studies have begun.[21-25]

The exploitation of such a technology necessitates being able to monitor both reaction steps to obtain optimum yields and cycling without deactivation, which occurs either by the irreversible solid-state transformation of the material or by coking. In the first step, it is crucial to avoid the formation of coke, since it cannot be eliminated or, if it is, it leads to the systematic pollution of H_2 produced by CO or CO_2. From this standpoint the nature of the solid and reactions conditions are important and will determine the viability of the cycling process. Furthermore, it is essential to understand the reaction mechanisms taking place during the chemical looping.

In our previous works on chemical looping with ethanol as the reducer, we explored both the nature of the surface species formed over various spinel mixed oxides used as cycling materials during reaction and the related gas products by means of *in-situ* diffuse reflectance spectroscopy and mass spectrometry.[24,25] It was shown that the first step in ethanol transformation was common to all spinels and corresponded to a dehydrogenation to acetaldehyde; depending on the spinel, however, acetaldehyde can be either oxidized to acetates (nickel-based spinel) or mainly decomposed to CO and methane (cobalt-based spinel) or completely oxidized (magnetite).

Different materials showed that the composition of ferrite affects product distribution, albeit to a limited extent. In particular, it was found that magnetite and copper ferrite were producing more hydrogen and CO than cobalt and nickel ferrites; the latter produced a greater quantity of acetaldehyde and, in the case of nickel ferrite, of methane. These studies also showed that the spinel materials, after only two steps, were irreversibly transformed with the segregation of Co, Ni, and Cu metal oxides.[25,26] In the case of copper, segregation occurred already during the thermal treatment of the precursor, in the case of nickel it started with the reduction step, while in the case of cobalt it occurred during the re-oxidation step. Consequently, magnetite was chosen as the looping material for the current work. It gave good results during the longer tests and led to complete recovery after a complete cycle.

The present work aims at further exploring the phase transformation that undergo magnetite during the two steps of the chemical looping i.e. the anaerobic oxidation/decomposition of ethanol and the re-oxidation by water. The surface and structural changes that solids go through as a result of cycling were studied using various physical techniques such as X-ray diffraction, and Mössbauer spectroscopy. Special focus was placed on the phase transformation during a cycle using the former technique under *in situ* conditions at 450°C.

2. Experimental

Magnetite material was prepared by co-precipitation.[24] Two solutions of $FeSO_4 \cdot 7H_2O$ (1M) and $FeCl_3$ (0.5M) were prepared and added drop-wise to a NaOH (2M) solution, at 50°C. The pH of the resulting solution was higher than 11. Afterwards this solution was kept at 50°C under vigorous stirring for 3 h. The precipitate formed was separated by filtration under vacuum and washed several times with bi-distillated water. Materials were dried at 80°C for about 15 h and annealed under a N_2 flow at 450°C for 8 h.

The metal contents of solids were determined by atomic absorption (ICP) in Argon plasma. The spectrometer was a SPECTROLAME-ICP, by SPECTRO. After the reforming and re-oxidation step, the carbon contents of the solids were determined using a Thermo Scientific MAS 200R CHNS/Oxygen automatic elemental analyzer with autosampler. The measurement accuracy was about 0.3%. The surface area of the solids was measured by a Micrometrics ASAP 2020 instrument. Samples were first degassed under vacuum at 300°C for 3 h. By using the adsorption–desorption isotherm at -204°C, surface areas were calculated using the Brunauer-Emmett-Teller (BET) method. X-ray photoelectron spectroscopy measurements (XPS) were performed using a Kratos Axis Ultra DLD spectrometer. The base pressure in the analysis chamber was better than 5 Å~ 10^{-8} Pa. XPS spectra of Fe2p3/2, Fe2p3/2, O1s, and C1s levels were measured. Binding energies relative to the carbon 1s signal at 284.6 eV were corrected and the $Fe^{2+}/(Fe^{2+}+Fe^{3+})$ ratio was determined as previously described.[27]

The reducibility properties of the material were studied by temperature programmed reduction (TPR) using a TPD/RO catalytic surface analyzer by the Thermo Quest Company. Samples of about 0.2 mg were first placed into contact with the He flow in order to remove the adsorbed species. Subsequently, samples were placed into contact with a flow of 5% H_2/Ar (20 $ml.min^{-1}$), heated at a rate of 10°C.min^{-1} up to 650°C, and then maintained at this temperature for 1h. Hydrogen consumption, expressed in mmol of consumed H_2 per gram of ferrite, was determined by taking into account a calibration analysis performed with CuO.

X-ray diffraction (XRD) patterns were obtained using a Bruker D8 X-ray diffractometer (Cu Kα radiation λ = 1.54184 Å) and varying 2θ diffraction angles from 5° to 80° during measurements. *In situ* powder X-ray diffraction was performed using a Panalytical X'Pert Pro MPD diffractometer with specific equipment and CuKα radiation.[28] Spectra were recorded with 0.02°(2θ) steps over a 10-80° 2θ angular range with 10 s counting time per step. Samples were mounted in the controlled atmosphere (dry nitrogen flow) cell and heated at a rate of 5°C min^{-1} from room temperature to 450°C. Patterns were recorded under nitrogen flow after successive periods of time under ethanol feeding (1 min with 0.52 $ml.h^{-1}$ flow of 11% of ethanol in nitrogen) and 20-min stabilization. Patterns were fitted using Bruker TOPAS profile and structure analysis software using the Rietveld method and allowing phase identification and quantification as well as unit cell parameter refinement.

The Mössbauer spectrometer is a homemade apparatus described elsewhere.[29] Samples were pressed into pellets after a dilution with sugar to limit absorbance. Spectra were recorded at 25°C, using a 2 GBq ^{57}Co/Rh γ-ray source and a conventional constant acceleration spectrometer, which was operated in triangular mode. Isomer shifts (δ), given with respect to αFe, and quadrupolar (Δ) or magnetic splitting (H) were recorded with a precision of 0.02 $mm.s^{-1}$. The accuracy of the fits was judged on the basis of fitting procedure conversion and χ^2 values. Mössbauer spectroscopy has been used extensively to analyze pure or doped magnetite,[30,31] and – if equal free recoil fractions for all the various Fe species are detected – it allows the determination of both the composition and relative concentration of the constituting phases from the relative spectral areas.

Chemical looping was performed using an experimental set-up built in the laboratory. Reactants were introduced using syringe pumps with constant flow (0.5 ml.h^{-1} of 11 % ethanol in N_2 and 0.5 ml.h^{-1} of 29 % water in N_2) and a VALCO valve to permit the rapid switching from one flow to the other while sending it to the looping material (magnetite), which was kept in a glass reactor at 450°C. Ethanol and water consumptions and product formations were followed by mass spectrometry (APSEC QMS [prototype] by SRA Instruments) at the outlet of the reactor. Details on the analysis of the reaction products are reported elsewhere.[26]

3. Results and discussion

Characterization of the cycling material

The preparation protocol chosen for the magnetite samples included a final heat treatment at 450°C only. This temperature was chosen in order to obtain a crystallized compound while keeping a specific surface area equal to 85 m^2.g^{-1}. It was important to determine the physical-chemical properties of the material before its use for *in situ* studies during reduction and oxidation reactions, and also to validate it in the looping process. The prepared cycling material was characterized by X-ray diffraction, Mössbauer and X-ray photoelectron spectroscopy, and programmed thermo-reduction. The results obtained are shown in Fig. 1.

The diffractogram of the synthesized material corresponded to that of magnetite (ICSD 00-019-0629) (Fig. 1a). No other phase was detected. The particle size calculated from the fitting of the powder pattern was equal to 10 nm, which is in accordance with a specific surface area measured of 85 m^2.g^{-1}. These X-ray diffraction results were confirmed by Mössbauer spectroscopy (Fig. 1b). The ^{57}Fe Mössbauer spectrum showed two sextets, which were characterized by 48.6 and 45.5 T internal magnetic fields, respectively; the first one corresponded to the contribution of the magnetic hyperfine interaction of Fe^{3+} in A-sites and the second to that of $Fe^{2.5+}$ in the B-sites of the spinel structure (AB_2O_4). Magnetite – Fe_3O_4 – is a ferromagnetic iron oxide: some of its iron atoms occupy sites with tetrahedral coordination (A-sites) and others occupy sites with octahedral symmetry (B-sites). These sites were characterized by easily distinguishable Mössbauer signals. At room temperature, Fe^{2+} and Fe^{3+} ions in the octahedral sites exchanged electrons at the same hopping rate as shown by the corresponding Mössbauer lines for a single state ($Fe^{2.5+}$). The relative spectral area of the two sites had an intensity ratio B:A equal to 1.9, which is close to the theoretical one (2.0). The slight discrepancy may be due to a slight surface oxidation and/or to a non-stoichiometry of the magnetite and the electron transfer process between Fe^{2+} and Fe^{3+} ions on the B sites.

The XPS analyses of the magnetite sample were in agreement with literature reports, with binding energies of 710.1 and 724.1 eV attributed to Fe 2p3/2 and Fe 2p1/2 levels, respectively. However, the analysis of the spectrum in the Fe 2p region (Fig. 1c) showed a satellite line, which indicated the presence of a higher amount of Fe^{3+} than the stoichiometric

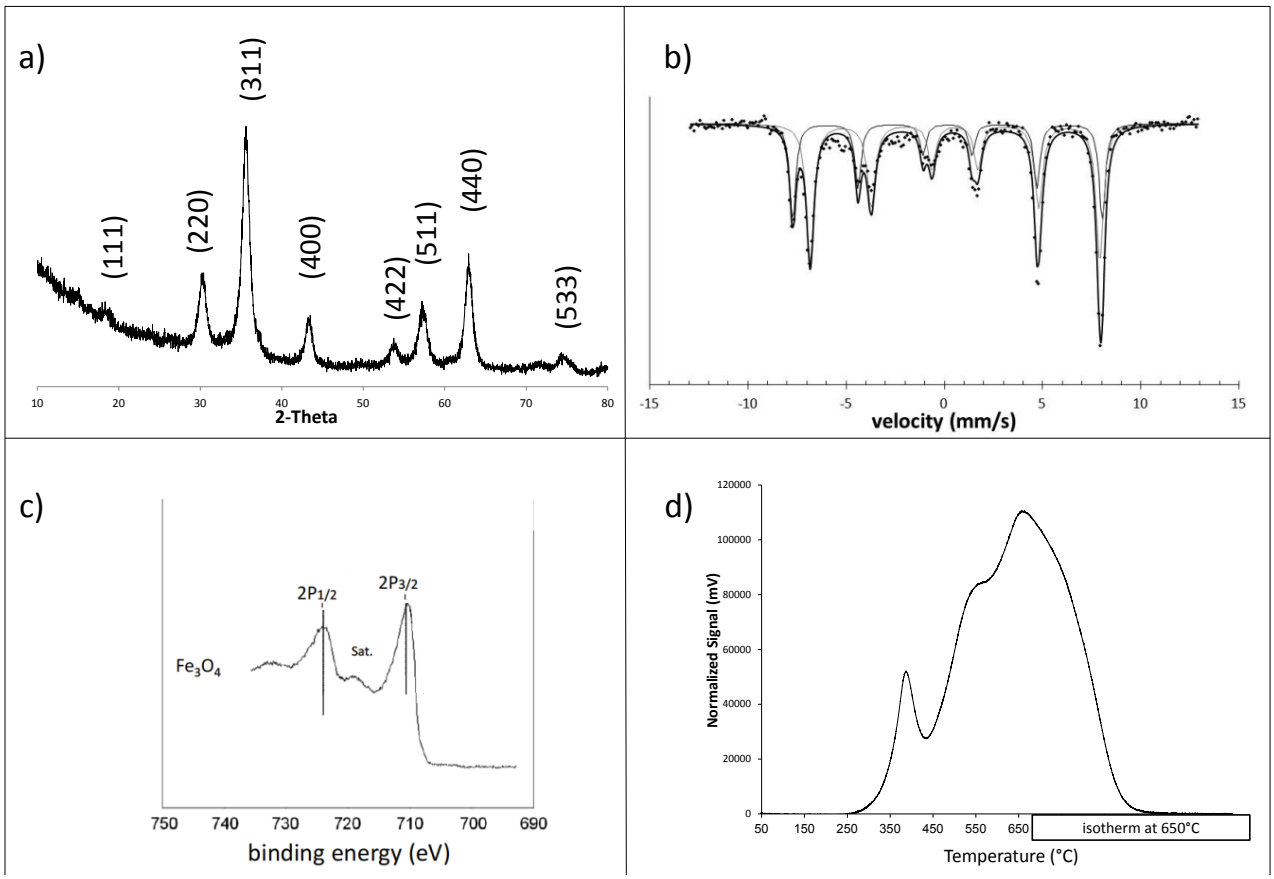

Figure 1: Characterization of the Fe_3O_4 annealed in N_2 at 450°C (a) XRD pattern, (b) Mössbauer spectrum recorded at 25°C (solid line is derived from least-square fit), (c) XPS spectrum of the Fe 2p region and (d) H_2-TPR profile.

one.[18] This might be explained by the presence of a surface impurity in FeOOH species which is related to a surface hydroxylation during the preparation or the storage of the material.[33]

The TPR profile of the material showed three main reduction peaks at 400, 550, and 650°C (Fig. 1d). The first peak was attributed to a low-temperature single-reduction pathway whereby FeOOH surface species are reduced:

$$6\ FeOOH + 4\ H_2 \rightarrow 2Fe_3O_4 + 4\ H_2O \qquad (1)$$

The other two largely overlapping peaks were much more intense and corresponded to the reduction of Fe_3O_4 occurring stepwise into FeO and Fe.[34]

We can see that, except for a slight surface oxidation, the material obtained corresponded well to magnetite and had the expected properties for further studies and, in particular, for an *in situ* X-ray diffraction study aimed at understanding the phase transformation occurring under ethanol and water during the two redox steps of the cycling.

In situ XRD study of the magnetite material

X-ray diffraction patterns in the magnetite sample were first recorded at 450°C under N_2 after successive ethanol and water feedings, as described in the experimental section. The patterns are presented in Fig. 1 and the results of their analysis in Fig. 2. Each of the calculated parameters was plotted as a function of the cumulative amount of ethanol to which the sample was exposed.

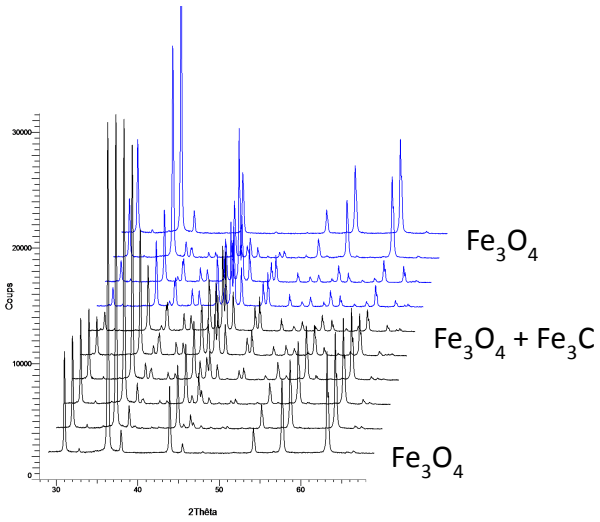

Figure 2: X-rays diffraction patterns of the looping material successively recorded at 450°C after pulsing ethanol (in black) and water (in blue).

No change in the phase composition was observed after feeding 0.15 mmol of ethanol (which, in the experiment conditions, corresponds to 1 minute of feeding). The magnetite should only be reduced in the surface or transformed in a very small amount. It should be remembered that X-ray diffraction is not extremely sensitive, and 1 or 2% of a new phase could easily go undetected. Furthermore, at the beginning, a small part of ethanol could be adsorbed on the walls of the *in-situ* cell and not pass through the powdered sample.

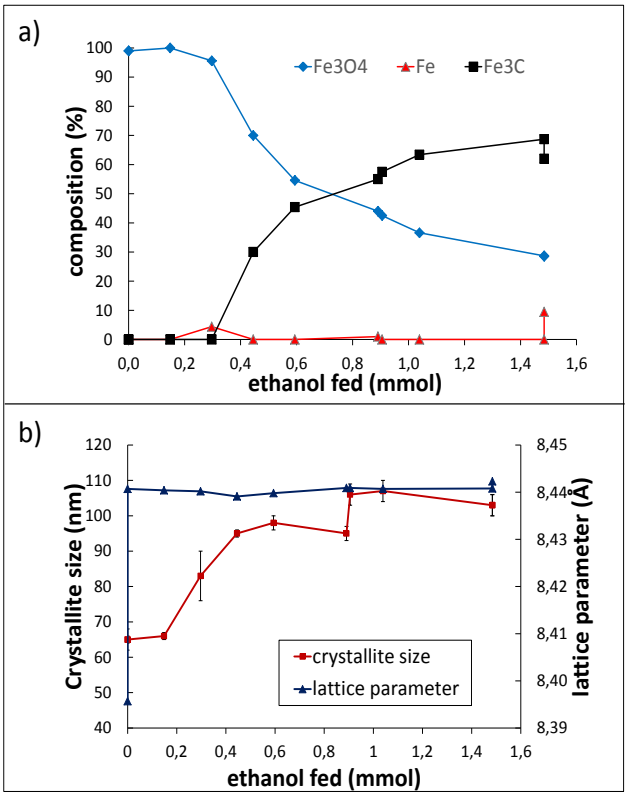

Figure 3: Variation of the sample composition (a) and of the magnetite crystallite size and unit cell parameter (b) as a function of the cumulative amount of ethanol flown on the sample at 450°C in the XRD in situ cell.

After feeding 0.30 mmol of ethanol a change was observed, with the formation of metallic iron αFe (ICSD 00-003-1050), representing 4% of the sample weight. The composition drastically changed when 0.45 mmol of ethanol were fed. At this point, the amount of magnetite decreased to 70%, while a new phase Fe_3C was formed and the iron phase previously seen disappeared. This clearly shows that the reduction of ferrite to iron carbides passes through the formation of metallic iron, which further reacts with deposited carbon to form Fe_3C. This is in accordance with what was suggested by Bonnet et al.[35]. With more feedings, the relative amount of Fe_3C continued to increase. In parallel, the magnetite phase underwent sintering with a mean crystallite size increasing from about 60 to 100 nm without changes in its cell parameter. The experiment was stopped after a total ethanol feeding corresponding to either 10 minutes of flowing ethanol or 1.5 mmol of ethanol. At that point, Fe_3C was the main phase and the phase composition did not undergo any further dramatic changes. The sample-containing chamber was then cooled down to room temperature under N_2 flow, for the night. The next day, the temperature was increased again up to 450°C, and a new pattern was recorded. The same pattern as that of the day before was expected: however, the composition of the phases changed slightly (first

item in Fig. 2a). The relative amount of magnetite was the same, but that of the carbide phase had decreased and a small amount of metallic irons appeared. It is possible that, during the process, the carbide decomposed to iron and C:

$Fe_3C \rightarrow 3Fe + C$ (2)

No peaks of C were found, but this could be due to both its low amount and the low crystallinity of the coke formed.

X-ray diffraction patterns in the magnetite sample were then recorded, again at 450°C under N_2, but after successive water feedings in order to study the re-oxidation of the material. This re-oxidation corresponds to the second stage of the chemical looping. The results are presented in Fig. 4.

The analysis of the patterns showed that both Fe and Fe_3C were rapidly and directly converted back to magnetite. The following equations may account for the main reactions taking place:

$Fe_3C + H_2O \rightarrow 3\ Fe + CO + H_2$ (3)

$Fe_3C + 2\ H_2O \rightarrow 3\ Fe + CO_2 + 2\ H_2O$ (4)

$3\ Fe + 4\ H_2O \rightarrow Fe_3O_4 + 4\ H_2$ (5)

The re-oxidation systematically stopped at magnetite and, in any case, Fe_2O_3 was not observed as could be expected from equilibrium thermodynamics.

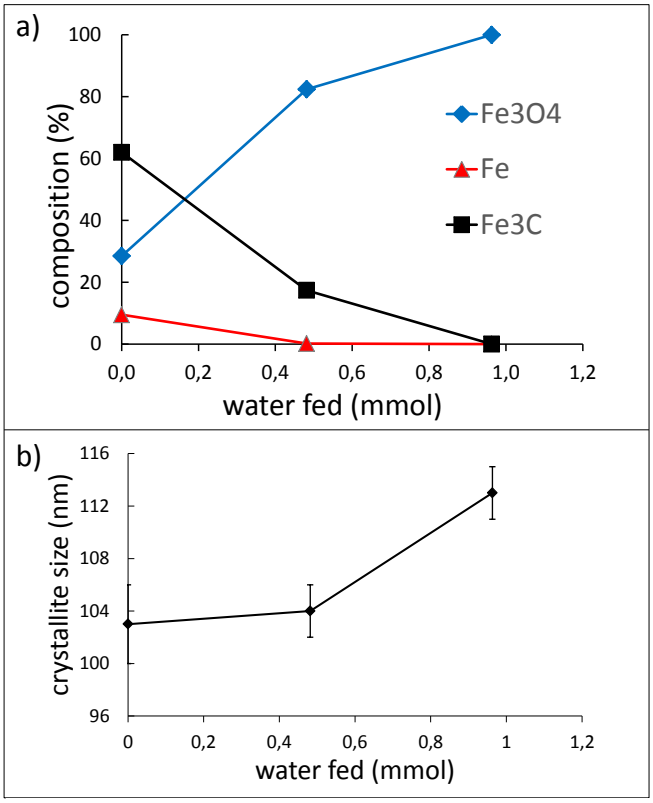

Figure 4: Variation of the sample composition (a) and of the magnetite crystallite size (b) as a function of the cumulative amount of water pulsed on the sample at 450°C in the XRD in situ cell.

The results obtained during the *in situ* XRD study show that at the beginning the magnetite is reduced to metallic iron, which is then converted into carbide following a progressive evolution, as already proposed in literature:[35-37]

Magnetite (Fe_3O_4) → [Wüstite (FeO)] → Iron (αFe) → Cementite (Fe_3C)

However wüstite, which is normally formed during the reduction of magnetite in metallic iron, as was the case during the TPR experiment, was never observed, and a doubt remains as to whether it was formed intermediately or not. Furthermore metallic iron is detected only at the beginning of the reduction process and in a very small amount, which may be explained by the existence of a second pathway corresponding to a direct conversion of iron oxide into carbide without the formation of metallic iron as proposed earlier.[35,38] In this case, the reduction should probably proceed through the formation of an oxi-carbide species, certainly amorphous and hard to differentiate from cementite via Mössbauer spectroscopy:

Magnetite (Fe_3O_4) → $Fe_xO_yC_z$ → Cementite (Fe_3C)

However, the results of the second stage in the *in situ* XRD study tend to confirm that the main pathway, taking place should well be the first one. If we consider this pathway, with the first fast reduction of magnetite into metallic iron, ethanol should rapidly adsorb on the metal surface formed where it dissociates. A super-saturation of the metallic phase with dissolved carbon may occur, and when the carbon activity in the metal is higher than the carbon activity for cementite (Fe_3C), cementite particles nucleate and grow on the metal surface and at the grain boundaries. Carbon diffusion is very slow through cementite and the latter should act as a barrier for a further carbon transfer from the gas phase to the metal one. This is why, after 10 min on stream, the phase composition observed during the *in situ* experiment no longer changed dramatically. This should consequently lead to the formation of graphite on the cementite surface. If this formation increases, the carbon activity increases at the graphite/cementite interface, which becomes unstable and starts decomposing according to equation (2). The formed metallic particles, which should not be present in large amounts, may be carburized but, most importantly, act again as catalysts for further carbon deposition.

This process explains in part the recorded formation of coke. It also explains why the coke formed has a tendency to grow as graphitic filaments. Indeed, when formed by the decomposition of carbide, iron particles are small and thus foster the formation of filaments when re-carburized. The analysis of the crystallite size in different phases showed that during the overall redox and transformation processes, all the phase crystallite sizes increased. In the case of magnetite, the sintering process appears independent of the reduction and transformation process, since it occurs at the same time during the first ethanol decomposition step, when it increases from 65 to 103 nm.

During the process of re-oxidation by water, the reduced magnetite is first transformed into metallic iron and then further oxidized to magnetite. The particle size of the formed magnetite continued increasing, but gradually, and did not exceed 120 nm. Most probably, the sample reached a sintering degree that was stable while it continued cycling. One of the major conclusions that can be drawn for a clean cycling process (without the formation of coke) might be that the formation of cementite

should be avoided. Nevertheless, it seems that this is impossible. However, it can be observed that no cementite was detected at the beginning of the step. It was thus interesting to run the looping process with a shorter cycling time.

Testing of magnetite in the short-time looping step process

In order to try to avoid the formation of cementite and, if possible, of coke in the first step of the chemical loop, we experimented short-time looping steps. To simulate a potential use of such an approach for the production of hydrogen, multi-cycle processes with steps of 5 and 2 min were run on a magnetite sample at 450°C. Moreover, this study made it possible to test the behaviour of the looping process over a long time, with continuous switching of the feeding, as well as to evidence any possible deactivation processes occurring over successive looping steps. With such short cycling times it was only possible to follow the consumption of ethanol or water and the formation of products by mass spectroscopy. The feeding was switched from C_2H_5OH/N_2 to H_2O/N_2, whereas the outlet gas mixture was analyzed continuously by mass spectrometry. In Fig. 4 the evolution of the number of ethanol moles is plotted as a function of time during 5- and 2-min step looping.

corresponding decrease in the specific surface area of magnetite, which was systematically evidenced at the beginning of the looping. Furthermore, both decreases were proportional to each other. Interestingly, ethanol conversion at the beginning of the cycling was total for about either 3 pulses of 5 min or 7 pulses of 2 min, which correspond approximately to the same amount of ethanol. This tends to confirm the X-ray study showing that the sintering occurs mainly during the reduction step.

In the example shown in Fig. 6, the hydrogen signal is shown over 6 consecutive loopings. The first part of the repeated signal (in yellow) represents the trend of H_2 obtained from ethanol, while the second part (in blue) represents that obtained from water. First, it can be observed that these signals are very stable. Reduction steps are those where hydrogen was formed in higher quantities (approximately 1.8 times more than for re-oxidation steps). A small peak in the H_2 signal can be observed at mid-cycle, just after the feeding of H_2O is turned on (Fig. 6). This small peak may be attributed either to the reforming of ethanol remaining in the tubes because of the absence of intermediate purge or to the "burn-off" of either carbon or the adsorbed species accumulated on the catalyst surface, which

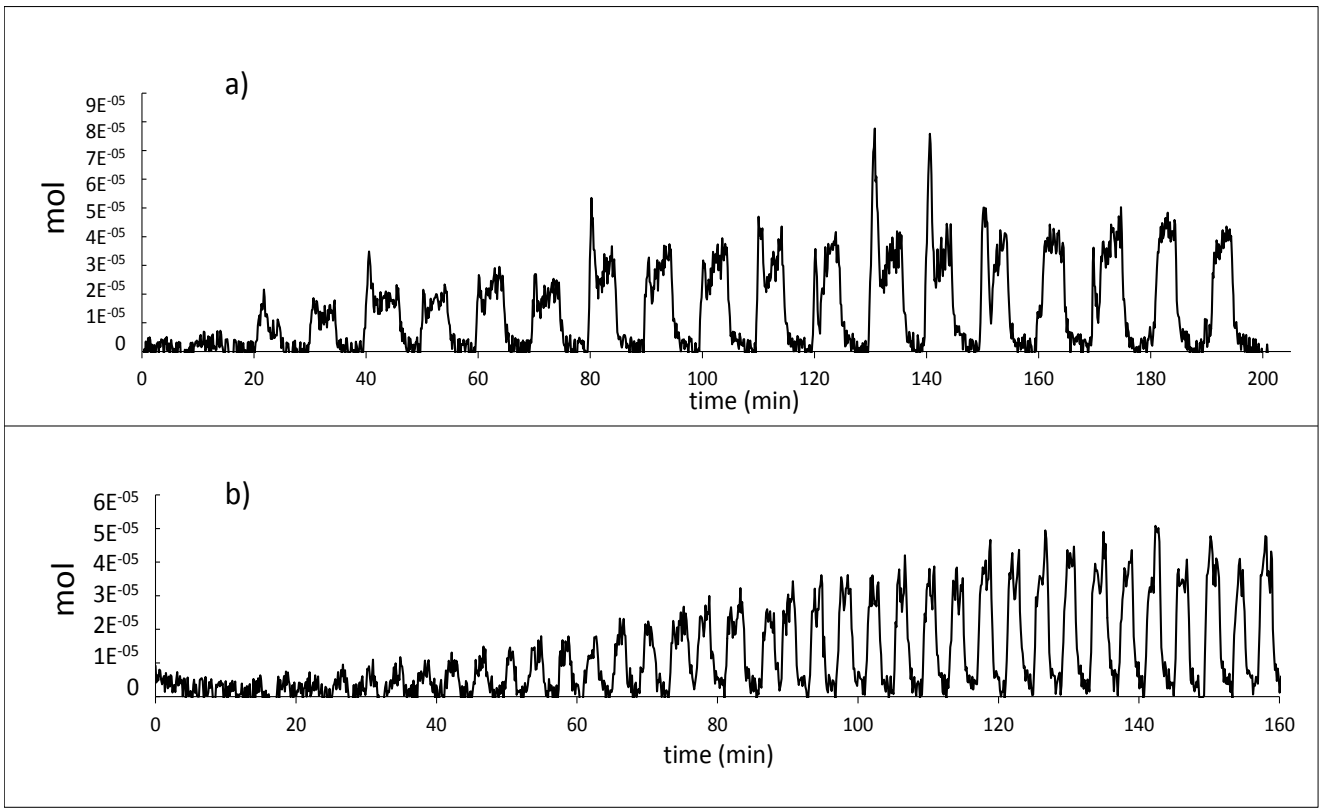

Figure 2: The evolution of ethanol mass spectrometry signal plotted as a function of time in 5 (a) and 2 min steps looping (b) In both case the cycling process was conducted on 0.4g of the magnetite sample at 450°C.

As can be seen, the conversion was similarly decreasing as a function of time over approximately 110 min, and then remained constant. This decrease may be explained by the increases the temperature slightly. After that initial period, the reaction is controlled by the diffusion of oxygen in the material. When the conversion was stabilized, the production of hydrogen during re-oxidation with water followed.

The quantity of H_2 produced per gram of magnetite during a 5 min step of re-oxidation has been calculated and was about 17 mmol H_2 which was slightly superior to the theoretical one (16.7 mmol). The slight excess of hydrogen could come from the re-oxidation of coke present on the reduced looping material.

It was not possible to identify all the products formed during reduction steps, but CO and CO_2 seemed to be the main by-products. CO and CO_2 were also detected during the re-oxidation step, which means that carbon species or coke are deposited on the material and are decomposed by water in the reaction conditions. In both cases CO_2 was the main product and the CO and CO_2 trends followed each other.

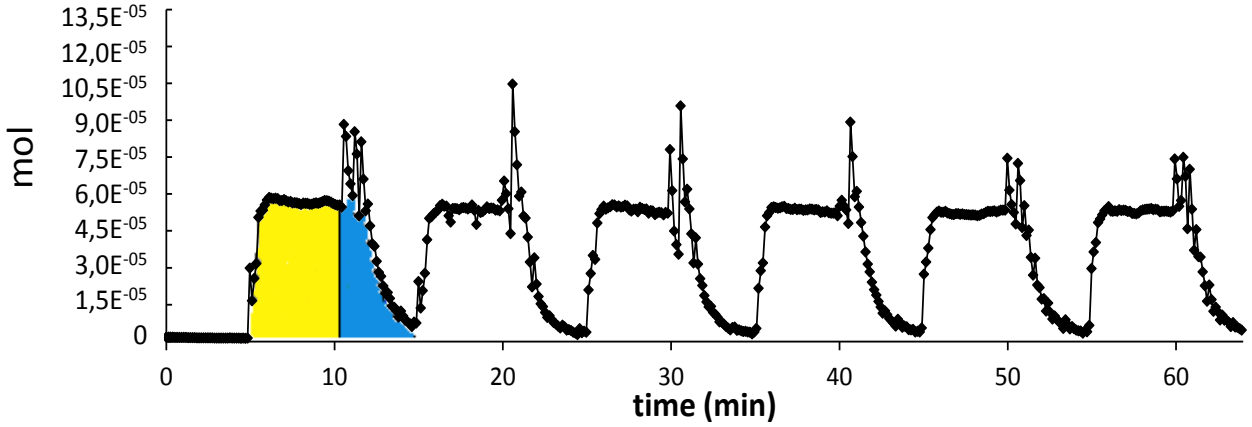

Figure 6: Evolution of hydrogen mass spectrometry signal plotted as a function of time in the cycling process was conducted on 0.4g of the magnetite sample at 450°C.

In a stable process, the material after cycling is the same as before. It was interesting to see what the maximum reduction/oxidation time ratio (R/O) that could be used in the cycling conditions chosen for the study was. In the 5-min step experiments, after the cycling became stable, the reduction time varied between 3 and 6 min, i.e. 0.6≤R/O≤1.2. The hydrogen mass spectrometry signals corresponding to the re-oxidation steps were recorded and the results of periodic cycling are shown in Fig. 7. As can be seen, the process cycles well up to a maximum R/O ratio of 1.0. At a higher value, the re-oxidation is not total (i.e. a 5-min re-oxidation step is not sufficient to re-oxidize the oxidation pathways the rate-limiting step should be the same and may correspond to the diffusion of oxygen species in a Fe_xO_y type phase. Thus it was important to understand the transformations taking place during the looping process, while the characterization of magnetite during the 5-min looping steps process was made.

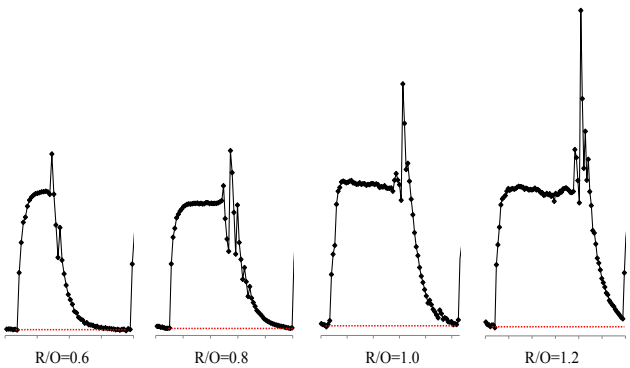

Figure 3: Evolution of hydrogen mass spectrometry signal plotted as a function of time in looping step with different reduction/oxidation time ratios on 0.4g of the magnetite sample at 450°C.

Characterization of magnetite during the short-time looping step process

The looping material was characterized by X-ray diffraction after various steps of the 5-min step looping experiment (Fig. 8). The patterns of the material at the end of the first and twentieth short-time cycles were similar to those recorded before the experiment and showed only one phase corresponding to magnetite. After the first and nineteenth reduction steps, the patterns were also similar, as they showed magnetite and small peaks corresponding to αFe. Only the intensity of the small peaks changed. No coke or carbide was detected. In order to better quantify the phases and detect the presence of minimal amounts of carbide and coke, Mössbauer analyses and elemental carbon analyses were performed. Fig. 9 shows the room temperature Mössbauer spectra of the Fe_3O_4 samples after the same steps of the short-time looping experiment. The hyperfine parameters calculated from the spectra are shown in Table 1.

The spectra before and after the complete looping are well fitted by the two identical magnetic sextets identified in the fresh material. Their relative spectral area was also the same. For spectra recorded after the reduction steps, a third sextet with an internal magnetic field of 32.6 T was observed. This sextet, with a systematically low spectral intensity (3-4%), might be attributed without ambiguity to αFe. Again, no trace

of iron carbide was observed. At the same time, the amount of coke adsorbed on the material was quantified (Table 1).

Table 1: Hyperfine parameters calculated from Mössbauer spectra recorded at 20°C (Fig. 7) with corresponding relative carbon weight content determined by chemical analysis.

Sample		Hyperfine parameters δ(mm/s)	H (T)	I (%)	Carbon content (wt. %)
After 5-min reduction	Fe^{3+}	0.26	48.8	34	0.3
	$Fe^{2.5+}$	0.65	45.8	63	
	Fe^{0}	-0.04	32.5	3	
After one cycle	Fe^{3+}	0.26	49.2	35	0.2
	$Fe^{2.5+}$	0.65	46.1	65	
After 19 cycles and 5-min reduction	Fe^{3+}	0.25	49.1	33	1.3
	$Fe^{2.5+}$	0.64	46.0	63	
	Fe^{0}	0.02	32.6	4	
After 20 cycles	Fe^{3+}	0.24	49.0	37	1.0
	$Fe^{2.5+}$	0.66	46.1	63	

δ: isomer shift, H: hyperfine field and I: relative spectral area.

It is interesting to note that the amount of carbon accumulated on the sample was very low. Carbon accumulated after the twentieth cycle was not proportional to the amount accumulated after the first cycle: it seemed likely that, with cycling, at least the same amount of carbon was deposited per step, whereas more was burnt at the re-oxidation step. It might be suggested that the carbon species that are rapidly burnt or not, respectively, correspond to aliphatic and aromatic carbon types.

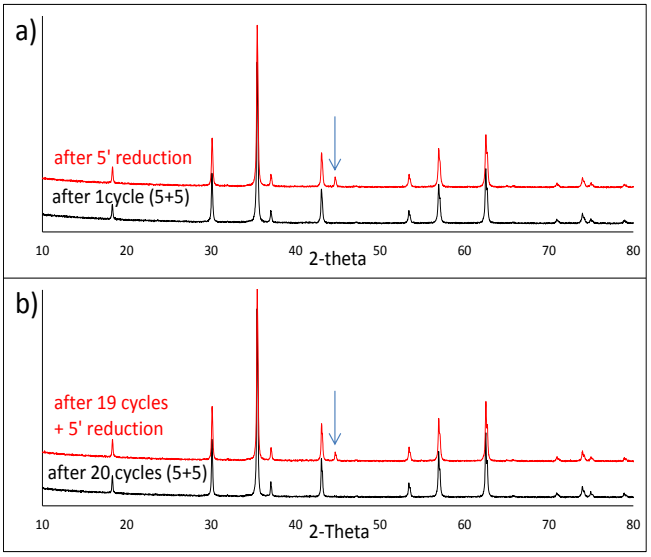

Figure 8: Comparison of the X-ray diffraction patterns recorded at room temperature before and after the re-oxidation step of the first short time cycle of 5 min (a) and before and after the re-oxidation step of the twentieth cycle short time cycle of 5 min (b). The blue arrow points to the main α Fe peak.

The latter might also correspond to either C in oxy-carbide species $Fe_xO_yC_z$, or a low-carbon iron phase Fe_xC_y formed during the reduction step.

The impact of the length of the cycling steps was apparent when comparing the amount of cementite – carbon deposited after a complete cycle with 2-, 5- and 60-min steps – with the amount of metallic iron formed after the first step of these cycles (see Table 2).

Table 2: Amount of coke adsorbed on the material, atomic % of iron in Fe_3C after complete cycling with different looping step lengths and atomic % of metallic iron after the first step.

Length of looping steps (min)	5	20	60
Amount of coke (wt %)	0.3	5.3	41.0
Amount of Fe in Fe_3C (at. %)	0.0	28.0	60.0
Amount of metallic Fe (at. %) after first step	4.0	0.0	0.0

We can see that short-time steps are needed to avoid the formation of cementite, but the formation of coke could not be avoided at any step time. Indeed, if the amount of coke in weight % (Cc) accumulated over the material is plotted as the reduction step duration time (t), it can be seen that it increased continuously following an equation of the type:

$C_c = \alpha\, t^n$ (6)

with α=9.009, n=0.503 and a correlation coefficient greater than 0.0999. This type of correlation is the same as that reported in Voorhies' earliest work, where coke formation was empirically described.[39]

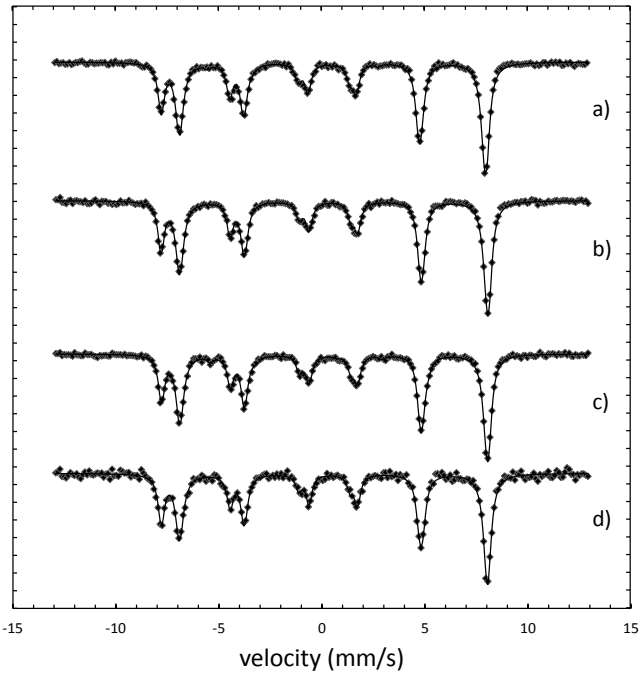

Figure 9: Experimental Mössbauer spectra recorded at room temperature of magnetite before (a) and after (b) the re-oxidation step of the first short time cycle of 5 min, and before (c) and after (d) the re-oxidation step of the twentieth cycle short time cycle of 5 min. Solid lines are derived from least-square fits.

Conclusions

In this work, we studied magnetite as a cycling material for the production of hydrogen by a chemical loop process using

ethanol and water as reducing and oxidizing agents, respectively.

The results of the *in situ* XRD study of magnetite under ethanol and then water at 450°C showed that magnetite was reduced into metallic iron and then converted into carbide. However, a direct parallel pathway for the transformation of magnetite to carbide is probable in a reducing and carburizing atmosphere. In this case, the reduction case should be achieved through the formation of unidentified oxi-carbide species. We showed that the carbide formed (cementite) was not stable and could decompose to iron and C and, similarly, catalyzed the growth of graphitic filaments and increased the rate of coke deposition. Thus it appears essential to avoid the formation of iron carbide during chemical looping. Through our *in situ* experiments we were able to show that the formation of cementite was postponed slightly at the beginning of the reduction step, and that by using short-time reduction it was possible to avoid the formation of cementite entirely.

We also proved that a stable cycling process may be used to produce hydrogen using short-time step cycles (up to 5-min steps). A complete recovery of the initial cycling material was possible, with only a slow accumulation of coke taking place with time over during cycling conditions. This deposited coke was limited to 1.0 wt % after 20 cycles (or 100 min). Thus, a third step to burn the coke left over by air will have to be periodically added for a sustainable industrial process, unless a cycling material and/or conditions totally avoiding the formation of coke are found. If it is not possible to achieve this goal, another challenge might be that of understanding the nature of the carbon species that are burnt and remain untransformed during the re-oxidation step by water, as well as of finding the way to encourage the formation of the latter. In such a case, the periodic regeneration of the material in air would not be avoided, but the hydrogen formed during the re-oxidation would be free from carbon oxides.

Acknowledgements

We gratefully acknowledge “Fondation Tuck”, Rueil-Malmaison Cedex (F), project Enerbio, 2011 for financial support. We also thank C. Lorenz for help in determining the carbon content of the studied materials and in setting up the chemical looping system.

Notes and references

[a] Dipartimento di Chimica industriale “Toso Montanari”, Università di Bologna, Viale Risorgimento 4, 40136 Bologna, Italy; E-mail : fabrizio.cavani@unibo.it; Fax: (+39)512093675; Tel: (+39)512093680.
[b] Institut de Recherches sur la Catalyse et l’Environnement de Lyon, CNRS, 2 avenue A. Einstein, F-69626 Villeurbanne Cedex, France ; E-mail :jean-marc.millet@ircelyon.univ-lyon1.fr; Fax: (+33)472445399; Tel: (+33)472445317.

Electronic Supplementary Information (ESI) available: [details of any supplementary information available should be included here]. See DOI: 10.1039/b000000x/

1 M. Bleeker, S. Gorter, S. Kersten, L. Ham, H. den Berg, H. Veringa, *Clean Technol. Environ. Policy*, 2010, **12**, 125.
2 H. Imanishi, A. Maeda, T. Maegawa, S. Matsuno, T. Aida, *Chem. Eng. Sci.*, 2008, **63**, 4974
3 K. Go, S. Son, S. Kim, *Int. J. Hydrogen Energy*, 2008, **33**, 5986.
4 D. Barrett, *Ind. Eng. Chem. Process Des. Dev*., 1972, **11**, 415.
5 J. de Wiebren, in *Hydrogen Fuel*, CRC Press, 2008, pp. 185–225.
6 V. Hacker, G. Faleschini, H. Fuchs, R. Fankhauser, G. Simader, M. Ghaemi, B. Spreitz, K. Friedrich, *J. Power Sources*, 1998, **71**, 226.
7 P. Salatino, O. Senneca, *Ind. Eng. Chem. Res*. 2009, **48**, 102.
8 F. Li, L.S. Fan, *Energy Environ. Sci*., 2008, **1**, 248.
9 J. P. E. Cleeton, C. D. Bohn, C. R. Müller, J. S. Dennis, S. A. Scott, *Inter. J. Hydrogen Energ*., 2009, **34**, 1.
10 E. R. Monazam, R.W. Breault, R. Siriwardane, D.D. Miller, *Ind. Eng. Chem. Res*. 2013, **52**, 14808.
11 O. Mihai, D. Chen, A. Holmen, *Ind. Eng. Chem. Res*., 2011, **50**, 2613.
12 A. Murugan, A. Thursfield, I.S. Metcalfe, *Energy Environ. Sci*., 2011, **4**, 4639.
13 Y. A. Daza, R. A. Kent, M. M. Yung, J. N. Kuhn, *Ind. Eng. Chem. Res*. 2014, **53**, 5828.
14 X. Ping Dai, J. Li, J. Tao Fan, W. S. Wei, J. Xu, *Ind. Eng. Chem. Res*. 2012, **51**, 11072.
15 C. D. Bohn, C. R. Müller, J. P. Cleeton, A. N. Hayhurst, J.F. Davidson, S. A. Scott, J. S. Dennis, *Ind. Eng. Chem. Res*. 2008, **47**, 7623.
16 M. Kierzkowska, C. D. Bohn, S. A. Scott, J. P. Cleeton, J.S. Dennis, C. R. Müller, *Ind. Eng. Chem. Res*. 2010, **49**, 5383.
17 D. Bohn, J. P. Cleeton, C. R. Müller, S. Y. Chuang, S. A. Scott, J. S. Dennis, *Energy Fuels* 2010, **24**, 4025.
18 F. Li, Z. Sun, S. Luo, L. S. Fan, *Energy Environ. Sci*., 2011, **4**, 876.
19 W. Liu, J. S. Dennis, S. A. Scott, *Ind. Eng. Chem. Res*. 2012, **51**, 16597.
20 A. Thursfield, A. Murugan, R. Franca, I. S. Metcalfe, *Energy Environ. Sci*., 2012, **5**, 7421.
21 V. Crocellà, F. Cavani, G. Cerrato, S. Cocchi, M. Comito, G. Magnacca, C. Morterra, *J. Phys. Chem. C*, 2012, **116**, 14998.
22 R. Campo, P. Durán, J. Plou, J. Herguido, J. A. Peña, *J. Power Sources*, 2013, **242**, 520.
23 E. Hormilleja, P. Durán, J. Plou, J. Herguido, J. A. Peña, *Int. J. Hydrogen Ener*, 2014, **39**, 5267.
24 C. Trevisanut, M. Mari, J. M. M. Millet, F. Cavani, *Int. J. Hydrogen Ener.*, 2014 *submitted for publication*.
25 J. Velasquez Ochoa, C. Trevisanut, J. M. M. Millet, G. Busca, F. Cavani, *J. Phys. Chem*. C, 2013, **117**, 23908.
26 S. Cocchi, M. Mari, F. Cavani, J. M. M. Millet, *Appl. Catal. B: Environmental*, 2014, **152-153**, 250.
27 J. M. M. Millet, M. Signoretto, P. Bonville, *Catal. Lett.*,2000, **64**,135.
28 B. Deniau, G. Bergeret, B. Jouguet, J. L. Dubois, J. M. M. Millet, *Top. Catal*., 2008, **50**, 33.
29 J. M. M. Millet, C. Virely, M. Forissier, P. Bussière, J. C. Vedrine, *Hyperfine Interac*., 1989, **46**, 619.
30 G. A. Sawatzky, J. M. D. Coey, A. H. Morrish, *J. Appl. Phys*., 1969, **40**, 1402.
31 Lima Junior, J. M. M. Millet, M. Aouine, M. do Carmo Rangel, *Appl. Catal. A: General*, 2005, **283**, 91.

32 T. Yamashita, P. Hayes, *Appl. Surf. Sci*., 2008, **254**, 2441.
33 T. Kendelewicz, T, P. Liu, C.S. Doyle, G.E. Jr Brown, E.J. Nelson, A. Chambers, A. Scott, *Surface Sci*., 2000, 453(1-3) 32.
34 W. Ramadan, M. I. Zaki, N. E. Fouad, G. A. H. Mekhemer *J. Magn. Magn. Mater*., 2014, **355**, 246.
35 F. Bonnet, F. Ropital, P. Lecour, D. Espinat, Y. Huiban, L. Gengembre, Y. Berthier, P. Marcus, *Surf. Interface Anal.*, 2002, **34**, 418.
36 W. K. Jozwiak, E. T. Kaczmarek, P. Maniecki, W. Ignaczak, W. Maniukiewicz, *Appl. Catal. A: General*, 2007, **326**, 17.
37 D. B. Bukur, X. Lang, J. A. Rossin, W. H. Zimmerman, M. P. Rosynek, E. B. Yeh, Ch. Li, *Ind. Eng. Chem. Res*., 1989, **28**, 1130.
38 O. J. Wimmers, P. Arnoldy, J. A. Moulijn, *J. Phys. Chem*., 1986, **90**, 1331.
39 A. Voorhies, *Ind. Eng. Chem*., 1945, **37**, 318.